

# Signatures of Cosmic Strings in the Cosmic Microwave Background

A. S. Lo & E. L. Wright

*UCLA Astronomy, PO Box 951562, Los Angeles, CA. 90095-1562 U.S.A.*

amy@astro.ucla.edu, wright@astro.ucla.edu

## ABSTRACT

We report a search for signatures of cosmic strings in the the Cosmic Microwave Background data from the Wilkinson Microwave Anisotropy Probe. We used a digital filter designed to search for individual cosmic strings and found no evidence for them in the WMAP CMB anisotropies to a level of  $\Delta T/T \sim 0.29$  mK. This corresponds to an absence of cosmic strings with  $G\mu \gtrsim 1.07 \times 10^{-5}$  for strings moving with velocity  $v = c/\sqrt{2}$ . Unlike previous work, this limit does not depend on an assumed string abundance. We have searched the WMAP data for evidence of a cosmic string recently reported as the CSL-1 object, and found an “edge” with  $2\sigma$  significance. However, if this edge is real and produced by a cosmic string, it would have to move at velocity  $\gtrsim 0.94c$ . We also present preliminary limits on the CMB data that will be returned by the PLANCK satellite for comparison. With the available information on the PLANCK satellite, we calculated that it would be twice as sensitive to cosmic strings as WMAP.

*Subject headings:* (cosmology:) cosmic microwave background

## 1. Introduction

Topological defects have been proposed as large scale structure (LSS) candidates but have fallen out of favor due to the lack of evidence for their existence. Topological defects form as results of phase transitions, many of which occurred in the first year after the big bang. They were ideal LSS candidates for three reasons. First, defects reflect the energy scale of the phase transition, therefore, the earlier the phase transition, the higher the energy density of the topological defect, and the larger the gravitational potential well for structure formation. Second, these high energy phase transitions occurred a long time before observational evidence of the first stars and galaxies. This would give gravity enough

time to coalesce material to form structures. Last, cosmic strings, the most popular class of topological defects, are geometrically similar to the filamentary LSS first observed in deep redshift surveys (see e.g. Vachaspati 1986).

However, despite these attractive features, results of the COsmic Background Explorer (COBE), an all-sky Cosmic Microwave Background (CMB) satellite, showed that cosmic strings were not responsible for large scale structure formation, because the CMB anisotropies were consistent with a Gaussian signature, while numerical simulations of all topological defects show that they would leave distinct non-Gaussian signatures in the CMB (see, e.g., a review by Allen et al. 1997). The COBE results were interpreted to mean that the observed LSS's are products of perturbations with Gaussian seeds, and cosmic strings fell out of favor as a structure formation mechanisms.

To date, there does not exist any conclusive observational evidence of the existence of cosmic strings or any other topological defect such as magnetic monopoles. On the other hand, CMB data do not preclude their existence in small enough numbers such that they do not appreciably affect the CMB angular power spectrum. There could be on the order of a few cosmic strings in the sky and they would not contribute enough power to significantly alter the CMB angular power spectrum (for recent cosmic string searches, see e.g. Perivolaropoulos 1998). Furthermore, topological defects are necessary products of certain types of phase transitions in the early universe, and are useful as possible explanations for variety of phenomenon such as Gamma Ray Bursts (e.g. Berezhinsky et al. 2001). This persistent interest in topological defects motivated our search for rare cosmic strings.

If cosmic strings do exist, they need to be either few in number, or have a small linear mass density. With that in mind, the current project performed a search for individual cosmic strings based on an all-sky CMB survey data. The data returned from the Wilkinson Microwave Anisotropy Probe (WMAP) have an angular resolution of 13 arc-minutes which enabled searches for individual cosmic strings, as 2 degrees is the scale at which we expect to see cosmic strings (see section II). While maps with greater resolution have been produced by balloon-borne experiments (e.g. Bouchet, Peter, Riazuelo, & Sakellariadou 2002), these experiments only observe a very small area of the sky. WMAP covers the entire  $4\pi$  steradian of sky and is therefore uniquely suited for searches of rare cosmic strings. Our search involves a pixel by pixel filtering, as opposed to the wavelet analysis that some others have performed on the small scale CMB experiments (e.g. Barreiro & Hobson 2001, Starck et al. 2004), although the underlying principles of searching for non-Gaussian signatures are similar.

## 2. Topological Defects

We are particularly interested in using cosmic strings as discriminators of the validity of Grand Unification Theories (GUT). GUTs have their roots in the successes of the electroweak union. The Glashow-Weinberg-Salam theory (Weinberg 1967) showed that electromagnetism and the weak force are united at energies slightly larger than the masses of their force mediators. The mass of the  $W$  boson is 81.4 GeV, the mass of the  $Z$  boson is 91.1 GeV and the photon is massless (Hagiwara et al. 2002). The current Standard Model of particle physics describes the universe well up to the electroweak unification, which occurred  $\sim 10^{-10}$  seconds after the Big Bang. GUTs seek to extend the Standard Model to include unification with the strong force, and describe all forces (except gravity) as the result of one unifying theory. Under these theories, the universe went through a series of phase transitions at various critical energies as it cooled.

At each epoch where a phase transition happens there is the possibility of forming topological defects. The high energies involved in GUT phase transitions cannot currently be reproduced in experimentally, which resulted in a lack of theoretical constraints for GUTs. This fact partially accounts for the proliferation of these theories, very few of which produce testable results. Topological defects, however, are necessary products of certain types of phase transitions. Different phase transitions with different properties produce distinct topological defects. Even if one does not believe that a GUT can be constructed, the existence or absence of topological defects can still give us limits on the types of allowable phase transitions in the early universe, and therefore more information on the evolution of the fundamental forces at very high energies.

Cosmic strings are a class of topological defects which are 1-dimensional; they are created as either filaments which span the horizon, or as closed loops. Filamentous cosmic strings leave tell-tale gravitational signatures. The metric of a long string in cylindrical coordinates, to linear order in mass per unit length of the string,  $\mu$ , is given by,

$$ds^2 = dt^2 - dz^2 - (1 - h)(dr^2 + r^2 d\theta^2) \quad (1)$$

where  $h = 8\pi G\mu \ln(r/r_0)$ ,  $r_0$  is a constant of integration, and  $r = (x^2 + y^2)$ , where  $x$  and  $y$  are the Cartesian coordinates for a string lying along the  $z$ -axis (Vilenkin & Shellard 1994). In general,  $\mu$  is expressed as a dimensionless quantity,  $G\mu$ , and,

$$G\mu \sim \frac{\eta^2}{m_{pl}^2}, \quad (2)$$

where  $m_{pl}$  is the Planck mass, and  $\eta$  is the symmetry breaking energy scale at which the cosmic string was formed. This metric describes a conical space, which can be thought of as

a Euclidean space with a wedge removed. The angle of the removed wedge is given by,

$$\Delta = 8\pi G\mu. \tag{3}$$

Two photons traveling on either side of the wedge would seem to be bent towards each other, and so cosmic strings can act as gravitational lenses.

The electroweak symmetry breaking scale occurs at 100 GeV. An electroweak string would have  $G\mu \sim 10^{-34}$ ; a GUT scale string would have  $\eta \sim 10^{16}$  GeV, which gives  $G\mu \sim 10^{-6}$ . Therefore, knowing the masses of the strings can give us the energy scale of the phase transition that created them. Alternatively, the absence of strings would give an upper limit to the energy of phase transitions which must create cosmic strings. Numerical simulations have shown that strings could intersect and break off loops in a process called intercommutation; this way, strings do not dominate the energy density of the universe. The amount of intercommutation can be tuned so that infinite strings have many intersections. Closed loops can wiggle and emit gravitational radiation, which causes the loop radii to decrease. Eventually, within the lifetime of the universe, string loop radii can reach zero. This is their primary energy dissipation mechanism (see e.g. recent numerical simulations, Moore, Shellard, & Martins 2002) that prevents cosmic strings from dominating the energy-density of the universe. Therefore, even if we do not directly observe a cosmic string today, their formation is not ruled out.

Cosmic strings grow along with the horizon size, and because they are created with relativistic velocity, string wakes will span the horizon. At the epoch of last scattering (LS), the horizon has angular size  $\theta_H$  given by,

$$\theta_H \simeq z_{LS}^{-1/2} \sim 2^\circ. \tag{4}$$

These string wakes create disturbances in the matter contained within the horizon. Since the CMB freezes gravitational signatures at LS, we expect to find most of the signatures of cosmic strings in the CMB at the LS scale. However, different numerical simulations give different string densities and velocities and there is little agreement on the size and number of strings we should see in the sky. The one fact that all simulations agree on is that string wakes leave edge-like signatures in the CMB.

We emphasize that cosmic strings are necessary products of certain phase transitions. The detection of a string would certainly be very interesting, but the absence of these defects is equally telling. If we expect GUT scale strings to form, one defect would be created per causal horizon. This leads to a possibility of  $\sim 13000$  cosmic strings in CMB. The gravitational signatures of these strings will persist in the CMB even if the strings themselves have dissipated.

### 3. WMAP

Photons produced in the early universe, when the ambient temperature was high enough to keep hydrogen ionized, remained in equilibrium with the baryons and traced baryon density. At a red-shift of  $z \sim 1100$ , electrons and protons recombined and the universe became transparent to photons. These photons have redshifted as the universe expanded and we now observe them as the 3K Cosmic Microwave Background. The photons retained the gravitational signatures of the early universe density distribution, except when modulated by the Sunyaev-Zeldovich effect.

The primary effect of a cosmic string on the CMB is to create temperature anisotropies due to the wake of the moving string. Along a particular line of sight, the temperature anisotropy,  $\delta T/T$  induced across a string moving in the plane of the sky is given by,

$$\frac{\delta T}{T} = 8\pi G\mu\beta\gamma. \quad (5)$$

where  $\gamma$  is the Lorentz factor and  $\beta = v/c$  is the velocity of the string.

The Wilkinson Microwave Anisotropy Probe (WMAP) is the latest NASA satellite to measure the temperature anisotropies of the CMB (see the LAMBDA website for a complete list of publications and public release data products<sup>1</sup>). WMAP has two back-to-back Gregorian telescopes which observe two patches of the sky separated by  $141^\circ$ . A set of differencing assemblies obtains the temperature difference between the two patches. The final data product of WMAP is the CMB temperature anisotropy of the each pixel in the sky, except where there are microwave sources and the pixels are masked. These masked pixels include most of the Galactic plane, the Galactic bulge, and some scattered sources off the Galactic plane.

WMAP was launched on June 30, 2001, and arrived at its L2 orbit on Oct. 1, 2001. The first year data release in February, 2003, contained data taken by WMAP from Aug. 10, 2001 to Aug. 9th, 2002. WMAP is still taking data and is expected to last at least until 2005. The following work is based on the first year data. As more data are released in the future, the sensitivity of this project will be improved as the pixel noise is reduced by repeated observations.

WMAP observes the sky at 5 frequencies, from 23 to 94 GHz. Relevant WMAP characteristics are tabulated in Table 1. The data products released by the WMAP science team include the thermodynamic temperatures of each WMAP pixel at all 5 frequencies. We used the data from the 3 highest frequency bands (Q, V, W) in our analysis.

---

<sup>1</sup><http://lambda.gsfc.nasa.gov/product/map>

#### 4. String Search: The Edgfinder

For our string search, we used the WMAP map of temperature differences,  $\Delta T/T$ , of the full sky. At 13 arc-minute resolution, the WMAP sky is divided into  $12 \times 4^9$  pixels. WMAP uses the Hierarchical Equal Area isoLatitude Pixelisation of the sphere (HEALPix<sup>2</sup>, Gorski et al 1999) to pixelize the sky. We have designed a digital filter for the WMAP data in search of signatures of filamentous string wakes, and we named this filter the Edgfinder. The Edgfinder took an input pixel and defined a window with radius  $RAD$ . Each pixel within this circular window was assigned an  $[x, y]$  pair, with the input pixel at  $[0, 0]$ , and the rest of the pixels'  $x$ s and  $y$ s are the normalized (to  $RAD$ ) displacements from the input pixel. The y-axis was defined to be parallel to the line connecting the North and South Galactic poles. Our filter window was small enough that we could consider the sky inside to be flat. For each pixel within the window, the Edgfinder multiplied the filter value,  $F(x, y)$ , with the pixel temperature at  $[x, y]$  and stored the sum of this product for all pixels in the window at the position of the input pixel. Therefore, the output of this digital filter was a map where the value at each pixel was a sum of the effects of the filter on the surrounding pixels. We called this output the Edgfinder value map, EV for short.

For the WMAP data and associated simulations, the Edgfinder had an  $RAD = 1^\circ$  window in the sky, which corresponded to the size of the horizon at LS. This window had a radius of 18 pixels and usually contained 260 pixels in total. The filter value,  $F(x, y)$ , was designed to pick out edges in the sky aligned with the y-axis of the filter. The specific values of each of the filter was generated separately, because pixel centers were slightly offset from each other depending on the pixel latitude, and the edges of the filter were ragged due to the diamond grid of the HEALPix scheme. This, coupled with the fact that we only have 240 pixels in the window, meant that the sum of the filter values didn't always sum to a perfect zero. We therefore generated the filter values twice at each pixel: the first time to collect the excess,  $a$ , for each window, and the second time to distribute  $a$  evenly among the pixels. This forced every window to sum to zero exactly.

The filter values,  $F(x, y)$ , were given by,

$$F(x, y) = N(x \mp A) \times \exp\left(\frac{-1}{1 - r_n^2}\right) \quad (6)$$

the minus sign applied to pixels with  $x < 0$  and plus for  $x > 0$ ,  $A$  was the normalized height of the filter, and  $N$  was the total normalization factor for the filter, discussed later. The exponential smoothing function ensured that the filter is smoothed and compact. The

---

<sup>2</sup><http://www.eso.org/science/healpix/>

normalized radius,  $r_n$ , is  $r_n = \sqrt{x^2 + y^2}$ . This filter was designed to be insensitive to a constant background value in the window, so that

$$\int F(x, y) dx dy = 0. \quad (7)$$

The filter is also insensitive to gradients,

$$\int xF(x, y) dx dy = 0, \quad (8)$$

and the value of  $A$  was adjusted to ensure this. The Edgfinder is depicted in Figure 1 as a shaded surface plot with the  $z$  axis representing the filter value,  $F(x, y)$ . In addition, a plot of the cross section of the filter, is also shown.

The filter could be rotated in the sky to detect strings of different position angles with respect to the North-South Galactic alignment. This was achieved by rotating through an angle  $\alpha$  by altering the  $[x, y]$  values of a pixel to  $[x', y']$  by the following transformation,

$$\begin{pmatrix} x' \\ y' \end{pmatrix} = \begin{pmatrix} x \\ y \end{pmatrix} \begin{pmatrix} \cos \alpha & -\sin \alpha \\ \sin \alpha & \cos \alpha \end{pmatrix}. \quad (9)$$

The filter values are then generated with  $x'$  in place of  $x$  and  $y'$  in place of  $y$ . In most simulations, we ran the filter at 20 different  $\alpha$  values equally spaced between 0 and 180 degrees. This represented a shift through one pixel at the edge of the filter window, and should pick out edges aligned in all directions.

The characteristic Edgfinder behavior around a string horizon is depicted in Figure 2. In this figure, the top picture is a simulated input temperature map, where the dark disk is the simulated string horizon. The disk edges are fuzzy due to the noise added to the map (as a real string in the sky would be seen by WMAP). The bottom picture is the Edgfinder response to the input map. The Edgfinder was oriented North to South, and produced a “hot” signal when encountering a rising edge, and a “cool” signal when encountering a dropping edge. If we rotated the filter window by  $180^\circ$ , we would get the opposite signal, meaning that the sign of the EVs was not important, so we used absolute values in our statistics. Running through 20  $\alpha$  angles from 0 to  $180^\circ$  really represented running through 40  $\alpha$  angles from 0 to  $360^\circ$ .

Visible on the same figure are pale circular disks which indicate masked pixels in the WMAP data, usually where there were strong foreground microwave sources. These regions were not used in our simulations. We used the combined Kp0 and Kp2 masks (see Bennett et al 2003 for an explanation of the masks) which masked 1109593 out of 3145728 pixels (35.7%). If strings were partially blocked by masked pixels, the Edgfinder can still detect them, but

at a reduced sensitivity. We ran tests where strings were partially blocked by a mask, with 5 different exposure levels from 100% to 18%, where 100% indicated an unblocked string. These results are tabulated in Table 2. For strings which are more than 50% exposed, there were no differences in the peak EV compared to an unblocked string. For strings that are less than 50% exposed, the peak EV dropped off rapidly as the string centers moved behind the mask, but were still detectable, their EVs dropping to around 15% of an unblocked string. This test indicated that strings with centers located outside of a masked area will be picked up normally by the Edgfinder, and therefore the masks are not blocking more sky than their actual area.

The Edgfinder filter values,  $F(x, y)$ , were calibrated to give a response of Edgfinder value, EV, of 1 for a 1 mK input signal. For example, if the input CMB map had all its southern hemisphere pixels at 1 mK, and northern hemisphere pixels at 2 mK, the Edgfinder would return  $EV = 1$  for equatorial pixels, and  $EV = 0$  at other pixels. The normalization constant for the  $RAD = 1^\circ$  WMAP Edgfinder was  $N = 0.33$ . Due to fluctuations in the normalization and the excess value collection of the filter, the actual response varied between 0.97 and 1.08, but averaged to 1.0 across the equator. Strictly speaking, the EV is unitless, but for the sake of clarity, we will sometimes give it units of mK. Unless specifically mentioned, all temperature units in this paper are in milliKelvin.

We created a set of calibrators to verify the gain of the Edgfinder. The calibrating set contained edges, or string horizons, of various temperatures ranging from  $\Delta T/T = 1.1$  mK to  $\Delta T/T = 1$  nK. The results of the calibration are in Table 3. In most cases, the EV was the same magnitude as the input edge to within 2%; we are therefore confident that the Edgfinder had a linear response to the input string horizon over the range of pertinent input temperatures.

The size of the Edgfinder was chosen to match the most likely string size that we may be able to find. For WMAP, this was a problem since this scale was also where the CMB Gaussian anisotropy signals were the strongest. The response of the filter to  $\ell$  values from 1 to 1000 is plotted in Figure 3 for representative  $\alpha$  angles. The largest filter response was around  $\ell = 200$ ; the WMAP data indicated that the first Doppler peak of the CMB anisotropy angular power spectrum is located at  $\ell \sim 220$ . This was undesirable as we wanted to be insensitive to as much of the Gaussian signal as possible so we could focus on the non-Gaussian signals.

One easy solution would be to make the filter smaller. However, this is not feasible with WMAP data. At  $RAD = 1^\circ$ , there were 273 pixels in the filter; at  $RAD = 0.5^\circ$ , there would be only 69 pixels in the filter, spanning less than 10 pixels. This resolution was too coarse to run the Edgfinder. For now, we report results of our good enough filter while we work

on ways to eliminate the response at  $\ell \sim 200$ . One certain method is to wait until PLANCK data is available, and with the improved resolution, we will get 270 pixels in the filter at  $RAD = 0.5$ . This is discussed in Section 6.

#### 4.1. Simulated Maps

We knew from the calibrator set described in the previous section that the Edgfinder had a linear response to the input edge. We next needed to find out how the Edgfinder responded to noisy maps like the ones from WMAP. We anticipated that the Edgfinder would not be able to detect strings when the string horizon signals became swamped with noise. In order to find this limit, we produced simulated maps to quantify the behavior of the Edgfinder. Once we understood how the Edgfinder responded to maps containing strings of known magnitudes, we could then set detection limits of the Edgfinder for the WMAP data. Because they are so vital, we describe in detail how we generated the simulated maps:

1. Coefficients,  $C_\ell$ , of the CMB angular power spectrum were generated by CMBFAST using the cosmological constants derived from the WMAP experiment, a  $\Lambda$ CDM cosmology, given by:  $\ell_{max} = 1500$ ,  $\kappa_{max} = 3000$ ,  $\Omega_b = 0.044$ ,  $\Omega_c = 0.218$ ,  $\Omega_\lambda = 0.738$ ,  $H_o = 71.6$ ,  $T_{CMB} = 2.725$ ,  $Y_{He} = 0.24$ ,  $N_{\nu(massless)} = 3.04$ ,  $\tau_{LSS} = 0.099$ , and  $n = 0.955$  (Bennett et al 2003).

2. We used HEALPix associated software SYNFAST to generate a CMB map which matched the  $C_\ell$  generated in Step 1. SYNFAST generates random Gaussian fields on a sphere based on the input power spectrum (the  $C_\ell$ 's).

3. We added string horizons at various temperatures,  $T_s$ , into the map by adding the value  $T_s$  to circular regions within a string radius  $R_s$ .

4. We used HEALPix associated software SMOOTHING to convolve three beams with the map made in step 3. A W-Band map was made by convolving a 13 arc-minute Gaussian beam with the  $a_{lm}$ 's of the temperature map created at Step 3, and the map regenerated with the new  $a_{lm}$ 's. A V-Band map was made from the convolution of a 21 arc-minute beam, and a Q-Band map from a 32 arc-minute beam. For each map generated in Step 3, three maps convolved with beams appropriate for the three WMAP bands were made.

5. The 3, W-, V-, and Q-Band, maps were averaged to get the final SMOOTHed map. Noise was then added to the map with the following prescription: the  $\sigma_n$  for the noise of

each pixel was generated by combining the noise characteristics of the 3 WMAP bands,

$$\sigma_n = \frac{\sqrt{\sigma_Q^2 + \sigma_V^2 + \sigma_W^2}}{3} \quad (10)$$

where  $\sigma_Q$  is the pixel noise in the  $Q$  band,

$$\sigma_Q = \frac{\sigma_{Q,0}}{\sqrt{N_{Q,obs}}} \quad (11)$$

$$\sigma_V = \frac{\sigma_{V,0}}{\sqrt{N_{V,obs}}} \quad (12)$$

$$\sigma_W = \frac{\sigma_{W,0}}{\sqrt{N_{W,obs}}} \quad (13)$$

where  $N_{Q,obs}$  is the number of times the pixel had been observed by the WMAP satellite in the  $Q$  band;  $\sigma_{Q,0} = 2.211$ ,  $\sigma_{V,0} = 3.112$ ,  $\sigma_{W,0} = 6.498$  are the noise weights given by the WMAP team. The noise values were generated by a Gaussian random number generator with  $\sigma = \sigma_n$ . The reason for this noise prescription, and for the convolution with three beams in Step 4, was that the data we fed to the Edgfinder are a composite of data from the three WMAP bands  $Q$ ,  $V$  and  $W$ . Due to the SMOOTHING and the added noise, the final string horizon temperature was at a slightly different temperature than the initial  $T_s$ . We sometimes also report, for comparison, the average temperature of the final input horizon, which we designated  $T_f$ .

## 4.2. Edgfinder Limits

In all, 82 input simulated maps were made according to the prescription given in Section 4.1. Out of these, 15 of the input maps were baseline maps, where no string horizons were inserted. We called the EV output of these maps the No-String sets. The maximum EV of a the No-String sets indicated the maximum EV due to background signals (i.e., not from the strings). In other words, the No-String sets produced the noise limit; we considered anything above this limit to be signal. Both the CMBFAST generated CMB signal and noise are basically Gaussian random variables, so we needed to have a range of No-String sets in order to ensure we have proper coverage of the possible noise values. To this end, we created 15 No-String input maps.

We then created the 67 “Stringy” maps, which contained different number of string horizons with various sizes and temperatures. The input string horizon temperatures ranged from  $T_s = 1.0$  mK to 0.0001 mK, the inserted string radius,  $R_s$ , ranged from 1.0 to 4.0 degrees. Most maps were made with one inserted string, but one map contained as many

as 60. The Stringy maps are further divided into single and Multi maps, where Multi maps had more than 1 inserted string horizons. There are 16 Multi maps.

Comparison between the maximum EV (Max EV) of the Stringy and No-String sets will yield the input string value that gives a Max EV above the No-String limit. The No-String limit is given by the largest value of the Max EVs of the No-String sets. The average of the maxima of the 15 No-String sets was  $EV = 0.242$  mK; the largest of the 15 sets was  $EV = 0.269$  mK. We have plotted the Max EV of all single Stringy sets against the input string temperature,  $T_s$  in Figure 4. The No-String limits are plotted as the dashed and dotted horizontal lines. A blow up of the region around the No-String limit is in Figure 5. The data indicates that an input string horizon of 0.345 mK and cooler yielded similar Max EVs as the No-String sets. We can consider  $T = 0.354$  mK as one of the limits to the sensitivity of the Edgfinder. If we took this limit to be wakes formed by strings traveling at  $c/\sqrt{2}$  (the mean absolute velocity of strings from numerical simulations), according to Equation 5, we would have limits for the cosmic string at  $G\mu \lesssim 1.37 \times 10^{-5}$ .

This is the crudest but most robust method of obtaining the sensitivity limit of the Edgfinder. The problem posed by the Edgfinder was that we were looking for very small non-Gaussian features in a largely Gaussian data set. For an input string of  $R_s = 2^\circ$ , the number of pixels whose filter window contained the edge constituted 0.0087% of the total pixels. The binning of the EV set data resulted in the non-Gaussian signatures occurring in the edges of the histogram. To improve upon the Max EV limits, we needed a set of descriptive statistics that could pick out small non-Gaussian signals at the outer edges of a Gaussian function. We found the Edgeworth Series to be suitable for our purposes.

### 4.3. Edgfinder Limits from Edgeworth Coefficients

We have binned the EVs such that the cosmic string signals are in the wings of the distribution. Since the CMB background is Gaussian, and we are looking for small deviations from a Gaussian, it is natural to consider using a series involving the Gaussian function,  $\alpha(x) = \exp(-x^2/2)/\sqrt{2\pi}$ , and its derivatives to fit our distribution,  $dF$ . Such a series would have the form,

$$f(x) \sim \sum_{j=0}^{\infty} c_j H_j \alpha(x) \quad (14)$$

where  $c_j$ s are coefficients to the  $H_j$ s, which are the Hermite polynomials. The  $j^{th}$  Hermite polynomial is the polynomial resulting from the  $j^{th}$  derivation of the Gaussian function  $\alpha(x)$ .

The Hermite polynomials have a generating function,

$$H_j(x) = (-1)^j e^{x^2} \frac{d^j}{dx^j} e^{-x^2}. \quad (15)$$

The series of the form given in Equation 14 that we have chosen to use is the Edgeworth series. The Edgeworth series is an asymptotic expansion of a distribution as a function of the  $\alpha(x)$  and its derivatives. A full derivation of the Edgeworth series can be found in Kendall (1987), and discussions relevant to astrophysics can be found in e.g. Juszkievicz et al. (1995) and Blinnikov & Moessner (1998).

The general form of the Edgeworth series is given by,

$$f(x) = (E_1 + E_2 H_3 + E_3 H_4 + E_4 H_5 + E_5 H_6 + \dots) \alpha(x) \quad (16)$$

The coefficients of the series,  $E_n$ , are given in terms of the cumulants,  $\kappa$ , of the distribution,  $dF$ . The  $j^{\text{th}}$  cumulant is a linear combination of the  $j^{\text{th}}$  and lower order moments,  $\mu_j$ . We obtain the cumulants of our distribution from calculating the moments of the distribution,  $dF$ , by,

$$\mu_j = \int_{-\infty}^{\infty} (x - \bar{x})^j dF \quad (17)$$

where  $\bar{x}$  is the mean of the distribution. The relationship between cumulants and moments is given by,

$$\mu_r = \sum_{j=1}^r \binom{r-1}{j-1} \mu_{r-j} \kappa_j \quad (18)$$

where the bracket is the binomial bracket. The first seven non-zero Edgeworth series coefficient are,

$$\begin{aligned} E_1 &= 1 \\ E_2 &= \kappa_3/6 \\ E_3 &= \kappa_4/24 \\ E_4 &= \kappa_5/120 \\ E_5 &= (\kappa_6 + 10\kappa_3^2)/720 \\ E_6 &= (\kappa_7 + 35\kappa_4\kappa_3)/5040 \\ E_7 &= (\kappa_8 + 56\kappa_5\kappa_3 + 35\kappa_4^2)/40320. \end{aligned}$$

We tested the Edgeworth Series on the histogram of a perfect Gaussian distribution, for which we knew all  $E_n$  coefficients should be zero. We found that the biggest effect

on the coefficients was how quickly the edges of the Gaussian function went to zero. For example, in two trial runs we used 1 million random numbers to represent a normal Gaussian distribution, with zero mean and unit variance. The one run where we allowed the  $x$  variable to go to  $x = 16$ , generated zeros at a level of  $10^{-17}$ . The other run where we only allowed  $x$  to go to  $x = 3$ , had zeros on the level of  $10^{-8}$ .

This meant that we had to choose the same set of bins for every EV set instead of binning the data with bin-size set by the maximum and minimum of each distribution. We experimented with the number of bins to see what our bin-size should be. With too few bins, the non-Gaussian aspects of the distribution were hidden. With too many bins, the residuals ( $\sum(data - fit)$ ) increased from errors at the wings of the distribution, and since this was exactly the location of the non-Gaussian signals we wished to detect, we had to be cautious. With the number of bins from 500 and 1000, the variation in the coefficients generated were within 10%. The optimal number of bins turned out to be 574, which struck a balance between generating a good zero value for the perfect Gaussian case, as well as having enough room at the wings for the non-Gaussian signals. We binned the absolute value of the EV set for each of the simulated maps into 574 bins, with the uppermost bin at 0.3 mK. The upper bin was chosen because maps containing EV greater than 0.3 mK were well above the Max EV of the No-String set and therefore were already known to contain strings. Since we used the absolute value of the EVs, we mirrored the histogram across the  $y$ -axis to create a negative half for the distribution; the whole distribution was then normalized.

Due to the fact that we reflected the distribution across the  $y$ -axis, the histograms were completely symmetrical. This meant that the odd moments (even cumulants) were zero. Thus, we only needed to look at the odd Edgeworth coefficients;  $E_n$  where  $n$  is 3, 5, or 7. For our purposes, the 7<sup>th</sup> Edgeworth coefficient,  $E_7$ , was a good discriminator of whether a map contained a cosmic string horizon. We have included plots of the other coefficients,  $E_3$  and  $E_5$ , in Figure 6 and Figure 7 respectively; note that the  $y$ -axis of Figure 6 is on a log scale to include all data points. Compared to the  $E_7$  coefficient,  $E_3$  did not pick out as many points, so at best, it can be used as corroborating evidence. The  $E_5$  coefficient was similar to  $E_3$ , but it included more points.

Out of the 15 sets of No-String maps, the  $E_7$  coefficients ranged from  $6.51 \times 10^{-6}$  to  $-3.92 \times 10^{-6}$ . Inspection of  $E_7$  and other coefficients showed that there was a clear trend: the Stringy sets which contained hot string horizons produced bigger non-Gaussian tails that were picked up by  $E_7$ . The fact that the  $E_7$  coefficients of the No-String set were distributed around zero tells us that a small  $E_7$  indicated a lack of non-Gaussian features like those produced by a string horizon. It also indicated the magnitude at which the  $E_7$  coefficient can be considered noise. This was corroborated by the fact that the higher the  $T_f$ , the larger

and more positive the  $E_7$  coefficient. Therefore, we could use the No-String  $E_7$  values as a discriminator between maps with strings and maps without strings. We took the second largest No-String (14th out of 15)  $E_7$  value as our limit of the Edgfinder’s single string sensitivity, at  $EV = 5.06 \times 10^{-3}$  mK.

The type of map that produced the smallest  $E_7$  signals were maps with only one string horizon inserted. We made 66 maps of single string with input temperatures ranging from 1 mK to 1  $\mu$ K. The  $E_7$  coefficients and input string horizons for all sets are graphed in Figure 8. It shows clearly that a large and positive value of  $E_7$  is indicative of the presence of hot string horizons. Figure 9 is a blow up of the region around the No-String limit. String horizons with  $T_s > 0.27$  mK were clearly above threshold  $E_7$  value. At  $T_s = 0.260$  mK we encountered the first string horizon with  $E_7$  below the threshold. We therefore set  $T_f = 0.27$  mK as our 100% confidence level of string detection. Examining Figure 9, we can see that the  $E_7$  values mostly fall within the boundary defined by the maximum No-String and minimum No-String  $E_7$ , with a few peeking above the threshold. The scatter in the data is very constant. Therefore the limit of our detection is firm at 0.27 mK; all input strings cooler this threshold looks like noise to the Edgfinder. For a cosmic string moving at mean simulation velocity,  $\beta = 1/\sqrt{2}$  this corresponds to a  $G\mu = 1.07 \times 10^{-5}$  string.

#### 4.4. Multiple String Maps

17 simulated maps were made with multiple string horizons inserted in the map, ranging from 1 to 60 horizons and  $R_s$  ranging from 1 to  $4^\circ$ . The number of string horizons and their sizes are summarized in Table 4. The purpose of the multiple string sets were twofold, first to determine if multiple strings had a similar effect on the Edgeworth coefficients as the single strings, and if so, determine the number of weak strings needed to generate an  $E_7$  signal above the No-String discriminant. The Max EV and the  $E_7$  coefficients for the multiple sets are plotted as letters A to P, according to their set name in Table 4, in Figures 5 and Figure 9, respectively. The bold items in the table represent sets with  $E_7$  coefficients larger than the No-String limit.

From the results of Sets A to C, we can see that the Max EV of multiple string sets are generated by individual strings, and therefore from the Max EV alone, we cannot tell if there are more than one hot string in the data. However, the  $E_7$  coefficient of multiple strings are cumulative. This means that in a situation where we have a small Max EV, and a large  $E_7$ , we know that the sky contains multiple strings.

However, looking at the results of Sets D, E, and F, we can see that if the strings are

cooler than the detection threshold, their  $E_7$  signatures are small enough that a few strings (less than 10) will not show detection. It takes quite a few cool strings for the cumulative effect to show up. For very cool strings ( $T_s \sim 0.15\text{mK}$ ), it takes 20 input strings for the  $E_7$  coefficient to be above the threshold.

The size of the string has some effect on the coefficients, but it is secondary to the strength of the edge. Compare Sets D to J and G to K; these sets have similar number of input strings, and similar  $T_s$ , but Sets J and K have twice the  $R_s$ , which means 4 times the number of pixels. The  $E_7$  coefficients of the sets are similar and show little trend reflecting the change in inserted string size. Furthermore, consider Set L, where the inserted string had  $R_s = 1$  degree; this set had an  $E_7$  coefficient significantly above the detection threshold. Both these phenomenon point to the fact that the Edgefinder is most sensitive to the temperature jump at the edge of a string horizon, rather than the size of the string.

The results of the multiple string sets shows that the Edgefinder limit is firmly set at  $T_s \sim 0.27$  mK. We can detect cooler strings, but they need to be numerous: looking at sets M and N shows that we need more than  $\sim 10$  strings of 0.15 mK for a detection. For very cool strings at  $T_s < 0.03$  mK, the data is very noisy. The multiple strings sets indicated that the most important criterion for string detection is the temperature of the input string. If the string is above the detection threshold, within a reasonable range of sizes, it will be picked up by the Edgefinder.

## 5. WMAP Results

The WMAP data we ran through the Edgefinder is an average of the data in three of the WMAP bands: Q, V and W. We called this the QVW composite map. Pertinent statistics of the WMAP QVW composite map are in Table 5, including the Max EV and its  $E_7$  coefficient. The resulting EV set was binned in the same manner as the simulated maps. Comparing the QVW composite map and the No-String sets, the statistics are similar.

Looking at the results of the WMAP composite QVW data, the maximum EV is below the threshold set from the max EV of the No-String set, and is in fact, below the maximum EV of half of the No-String simulated data sets. This means that there are no hot string horizons in the WMAP data at the level of noise set by the No-String sets. The  $E_7$  coefficient leaves no doubt that there are no non-Gaussian signatures in the tail of the distribution of the WMAP data produced by string horizons similar to those we inserted into the simulated maps. We can confidently say that the Edgefinder did not find any evidence of string wakes in the CMB data measured by WMAP, to the single string limit of  $G\mu < 1.07 \times 10^{-5}$ . The

20 string limit of less 0.15 mK strings gives  $G\mu < 5.97 \times 10^{-6}$ .

We mention again the fact that in the actual WMAP data, due to Galactic and foreground contamination, about 1/3 of the pixels were masked. We have reproduced this masking in our simulated data so that we have the same number of pixels per map as the actual WMAP data. We caution that any strings hidden behind these masked pixels would not be picked up by the Edgfinder.

### 5.1. WMAP 2nd Year Simulation

We have performed the analysis necessary in anticipation of the WMAP second year data release. All of the analysis were done in the same manner as the first year data, with the exception that the noise is now  $1/\sqrt{2}$  time the noise of the first year data. The second year data has limits at max EV = 0.283 mK and  $E_7 = 0.257$  mK. The  $E_7$  threshold yields a single string limit of  $G\mu < 1.02 \times 10^{-5}$ . Most of the noise in our string search is due to the first acoustic peak in the CMB angular power spectrum; the Edgfinder is cosmic variance limited, so reduced radiometer noise has little effect.

## 6. A Cosmic String Candidate?

Sazhin et al.(2003) reported a discovery of an object which contains two sources of identical isophotes, color, and fitted 2-D light profiles in the Osservatorio Astronomico di Campodimonte Deep Field (OACDF). In addition, spectra of the sources are identical with a confidence level higher than 99%. Morphological arguments led them to propose that this object is a background galaxy lensed by a cosmic string. They have named this object the Campodimonte-Sternberg-Lens candidate 1, or CSL-1. The red-shift of both sources in the object is  $0.46 \pm 0.008$ ; the separation of the two sources is 2 ''.

Precise finder charts for the object were not available. We found this object by visually inspecting the OACDF deep field and comparing it to the Palomar All Sky Survey plates. We found CSL-1 to be located at (J2000) RA 12:23:30.72, Dec -12:38:57.8. There may be some small uncertainty about the location of CSL-1. We examine the WMAP data at this location to see if the Edgfinder can detect a string. As WMAP data had a resolution of 0.23 degrees, by including the four nearest pixels to that coordinate, we believe we have covered this object in our search.

### 6.1. String Search

From the image separation, we can derive a string mass per unit length,  $\mu$ . In a flat universe where  $\Omega_{matter} = 1$ , from Gott (1985), we find that the image separation  $\Delta\theta$  of lensing by a cosmic string is related to  $D$ , the deficit angle of the conical space around the string, by,

$$\Delta\theta = D \left[ \cos \alpha - \frac{1 - (1 + z_s)^{-1/2}}{1 - (1 + z_g)^{-1/2}} \right] \quad (19)$$

where  $z_s$  is the red-shift of the string,  $z_g = 0.48$  is the red-shift of the background object (galaxy), and  $\alpha$  is the angle of the straight string with respect to the plane of the sky. If we assume that the string is in the plane of the sky, which means  $\alpha = 0$ , there are two limiting results: for  $z_s = 0$ , we find  $\Delta\theta = D$ ; for  $z_s = 0.4$ ,  $\Delta\theta = 0.102D$ .

For a flat universe,  $D$ , is related to the string mass per unit length,  $G\mu$  by,

$$D = 8\pi G\mu. \quad (20)$$

Therefore, with a maximum  $D$  of  $9.7 \times 10^{-6}$  radians, we get  $G\mu = 3.86 \times 10^{-7}$ . A string will cause a jump in the value of the temperature of the CMB due to Doppler shifting. The change in temperature is given by Equation 5.

We have processed WMAP data at the position of the CSL-1 object and compared the Edgefinder values to Edgefinder values of regions with similar sky coverage and galactic latitude. The CSL-1 object was small enough that it was within one WMAP pixel (on pixel 968549). However, we include results from the surrounding 4 pixels in the event that we have misjudged the position of CSL-1. In addition, the alignment of the two images contains some uncertainty, thus we also ran the Edgefinder along two separate position angles,  $\alpha = 0$  and  $\alpha = \pi/20$ . The results are in Table 6.

The Edgefinder values of the 4 pixels are all above the 95th percentile, especially pixels 968548 and 968527, which have very high E.V.'s above 99th percentile. However, these high percentiles can be misleading. First, they are all significantly under the No-String detection limit. Second, as an upper limit, if we allow the WMAP temperature at those pixels to be entirely caused by the presence of a string, we can say that the EV is exactly the  $\Delta T$  due to the string motion, due to the Edgefinder gain being 1. With the  $G\mu$  given above, this means for an E.V. = 0.08686 mK, the string needs  $\beta\gamma \gtrsim 3.3$ , or  $v = 0.957c$ , to account for the temperature jump. The ranges of string velocity for the E.V. in Table 6 is from  $v = 0.941c$  to  $v = 0.979c$ . These high string velocities makes the case for the existence of cosmic strings at this location more unlikely, as the rms string velocity is  $v \sim 0.7c$ . We therefore cannot say that we have a significant detection of a cosmic string at the location of CSL-1 in the WMAP data.

## 7. Simulated PLANCK Results

Looking forward, we also made simulated maps of CMB data that will be gathered by European Space Agency’s PLANCK satellite. PLANCK is scheduled to launch in 2007. Most of PLANCK is still being constructed, so we do not have data on the noise characteristics of PLANCK. What we do know is that PLANCK will have a 5 arc-minute resolution, with a temperature sensitivity of  $4 \times 10^{-6}$  K (more information is available from the PLANCK website<sup>3</sup>). We expect PLANCK will have about 1/10 the noise of WMAP. For our simulated PLANCK maps, we followed the same procedure outlined in Section 4, except in step 5, where for the added noise, we used 1/10 the average WMAP noise value for the  $\sigma_n$  of each PLANCK pixel. In the HEALPix scheme, the improved PLANCK resolution means having 12 million pixels in the sky, a 4 fold increase on WMAP. Running each simulated map at 20  $\alpha$  angles became computationally infeasible. Therefore, we only ran the PLANCK maps through 6 different  $\alpha$  angles, spaced equally between 0 and 180°.

The increased resolution of the PLANCK satellite will allow us to bypass the problems of being sensitive to the first Doppler peak at  $\ell \sim 200$ . With the PLANCK Edgefinder at  $RAD = 0.5^\circ$ , we still had  $\sim 270$  pixels in the filter window, which was comparable to the number of pixels in the WMAP Edgefinder window of  $RAD = 1.0^\circ$ . The transfer function for the  $RAD = 0.5^\circ$  PLANCK Edgefinder filter is plotted in Figure 10. For the  $RAD = 0.5^\circ$  Edgefinder, the peak filter sensitivity is at  $\ell \sim 500$ , well away from the first Doppler peak. We performed the bulk of our simulation using the  $RAD = 0.5^\circ$  PLANCK Edgefinder. At this resolution, the PLANCK filter had a similar number of pixels as the WMAP  $RAD = 1^\circ$  filter, so the gain from the filter was comparable.

As with the WMAP set, we created calibrators for the PLANCK Edgefinder and tuned the filter to return  $EV = 1$  for a 1 mK edge. Noise-only,  $\Lambda$ -CDM-only maps were put through the PLANCK Edgefinder for calibration purposes. We made a total of 30 Stringy PLANCK maps with only one string horizon per map. In addition, 6 baseline No-String maps were generated. Since the range of EV for PLANCK is expected to be wider, the optimum number of bins for the PLANCK data is 704. The total number of data points remain similar to the WMAP simulation, so the comparison of the two statistics is valid.

The plots of the string temperature,  $T_s$ , of a map vs. the max EV, and vs.  $E_7$  are in Figure 11 and Figure 12, respectively. The limit obtained from the max EV was very similar to the the limit obtained from the  $E_7$  coefficient, most probably as a result of the fact that we have eliminated a lot of the Gaussian signal by going to a smaller Edgefinder

---

<sup>3</sup><http://www.rssd.esa.int/index.php?project=PLANCK>

window. This strengthened our confidence in these limits. Both the Max EV and  $E_7$  methods indicated that the detection limit for the PLANCK Edgfinder occurred at  $T = 0.14$  mK. This represented a factor of 2 increase in the single string Edgfinder sensitivity compared to the WMAP data. This is, however, very similar to the multiple strings limit for the WMAP data. For a cosmic string moving at mean simulation velocity,  $\beta = 1/\sqrt{2}$  this input string corresponds to a string mass of  $G\mu = 5.77 \times 10^{-6}$ .

## 8. Conclusions

We have constructed and calibrated a digital filter for the WMAP CMB data to search for cosmic strings. By comparing the WMAP data and a control set created from CMBFAST and SYNFAST, we have concluded that the CMB data returned by the WMAP satellite do not contain single strings to the limit of  $G\mu \lesssim 1.37 \times 10^{-5}$  using the max EV as the threshold, and  $G\mu < 1.07 \times 10^{-5}$  using the 7th Edgeworth coefficient as the threshold. This limit may be more stringent if we allow the sky to have multiple strings, to a limit of  $G\mu < 5.97 \times 10^{-6}$ , if there are more than 20 string horizons in the sky. We caution that WMAP effectively examined 2/3 of the visible sky, so it is possible that we are missing strings in our analysis. With the second year WMAP data, we can improve this limit by about 5%. This improvement is a result of an expected 30% improvement in the WMAP radiometer noise. However, because the Edgfinder filter window was 2 degrees, the first CMB doppler peak generated a large background that cannot be filtered out, and therefore a large reduction in radiometer noise generated a relatively small improvement in the discrimination threshold.

We have also investigated claims of a possible cosmic string detection of the object CSL-1, and found little evidence of a string at this position. For the proposed string mass of  $G\mu = 3.86 \times 10^{-7}$ , WMAP CMB temperatures at the location of CSL-1 would require the string to have been moving very relativistically, with  $v \sim 0.96c$ . We conclude that this is unlikely, and that much more sensitive and higher angular resolution data would be needed for a critical test of CSL-1.

We ran the Edgfinder through simulated PLANCK data. As more information about the PLANCK satellite becomes available, we can do a more realistic modeling of the noise characteristics and therefore get better limits on the strength of cosmic strings PLANCK can detect. Currently, we have a projected limit of  $G\mu \gtrsim 5.77 \times 10^{-6}$ , a factor of two better than the single string limit from WMAP. The predicted detector noise of PLANCK is too small to affect the filter appreciably, and the true limit of the PLANCK data for the Edgfinder is cosmic variance. The factor of two improvement over the first year WMAP data is mostly a result of the smaller filter window which reduced signals from the first CMB doppler peak.

With more and more sensitive all sky CMB surveys, we can begin to set firm experimental limits on the existence of GUT scale cosmic strings, and thereby limiting the types of allowed phase transitions.

We would like to thank the authors of CMBFAST U. Seljak and M. Zeldarriaga, and the creators of HEALPix (Gorski, Hivon, and Wandelt 1999).

## REFERENCES

- Allen, B., Caldwell, R. R., Dodelson, S., Knox, L., Shellard, E. P. S., & Stebbins, A. 1997, *Physical Review Letters*, 79, 2624
- Barreiro, R. B. & Hobson, M. P. 2001, *MNRAS*, 327, 813
- Bennett, D. P. & Bouchet, F. R. 1990, *Phys. Rev. D*, 41, 2408
- Bennett, C. L. et al. 2003, *ApJS*, 148, 97
- Berezinsky, V., Hnatyk, B., Vilenkin, A., *Phys. Rev. D* 64 3004B
- Blinnikov, S. & Moessner, R. 1998, *A&AS*, 130, 193
- Bouchet, F. R., Peter, P., Riazuelo, A., & Sakellariadou, M. 2002, *Phys. Rev. D*, 65, 21301
- Hagiwara, K. et al. 2002, *Phys. Rev. D*, 66 100001
- Gorski K. M., Hivon E., Benjamin D. Wandelt B. D. 1999, *Proceedings of the MPA/ESO Cosmology Conference: Evolution of Large-Scale Structure*, 37
- James, I. M. 1984, *General Topology and Homotopy Theory* (Springer-Verlag, New York, NY.)
- Juszkiewicz, R., Weinberg, D., Amsterdamski, P., Chodorowski, M., Bouchet, F., 1995, *ApJ*, 442, 39
- Kendall, M. 1987, *Kendall's Advanced Theory of Statistics* (New York, Oxford University Press)
- Moore, J. N., Shellard, E. P., & Martins, C. J. 2002, *Phys. Rev. D*, 65, 23503
- Ray, R., Srivastava, A. M. 2004, *Phys. Rev. D*, 69 103525
- Perivolaropoulos, L. 1998, *Phys. Rev. D*, 58, 103507
- Starck, J.-L., Aghanim, N., & Forni, O. 2004, *A&A*, 416, 9
- Vachaspati, T. 1986 *Physical Review Letters* 57.1655V
- Vilenkin, A., Shellard, E.P.S., 1994, *Cosmic Strings and other Topological Defects*, (Cambridge, UK, Cambridge University Press)
- Weinberg, S. 1967, *Physical Review Letters*, 19, 1264

---

This preprint was prepared with the AAS L<sup>A</sup>T<sub>E</sub>X macros v5.2.

Table 1. Relevant WMAP Characteristics

Frequency GHz	Resolution FWHM, arcmin	Wavelength mm	Sensitivity $\mu\text{K}, 0.3^\circ \times 0.3^\circ$
23	56	13.6	35
33	41	10.0	35
41	32	7.5	35
61	21	5.0	35
94	13	3.3	35

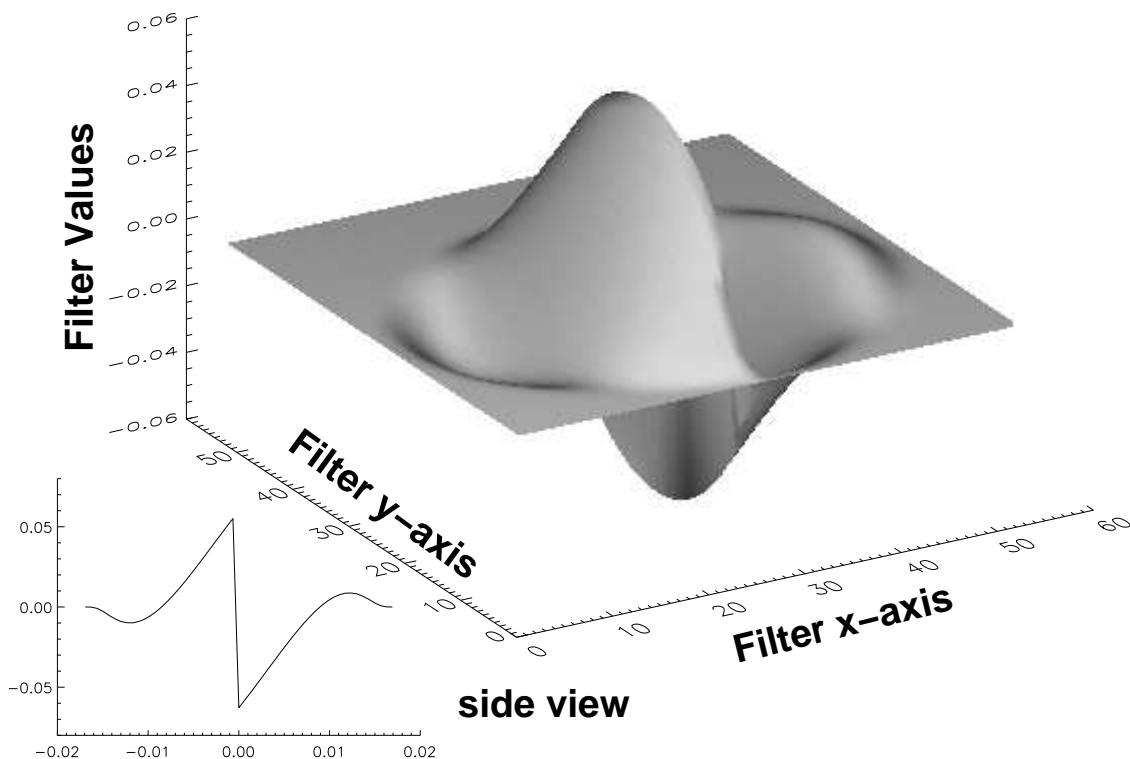


Fig. 1.— A 3-D representation of the Edgefinder. The z-axis represent filter values, and the x and y axis are the pixel numbers. The right bottom inset is a plot of the cross section of the filter, with the x-axis being the distance from the filter center, and not the pixel number.

Table 2. Partially Exposed Strings

Exposure %	Normalized Max EV	Non-zero Pixels
100	0.961	575
73.6	0.956	339
48.7	0.569	210
32.6	0.160	135
18.0	0.143	71

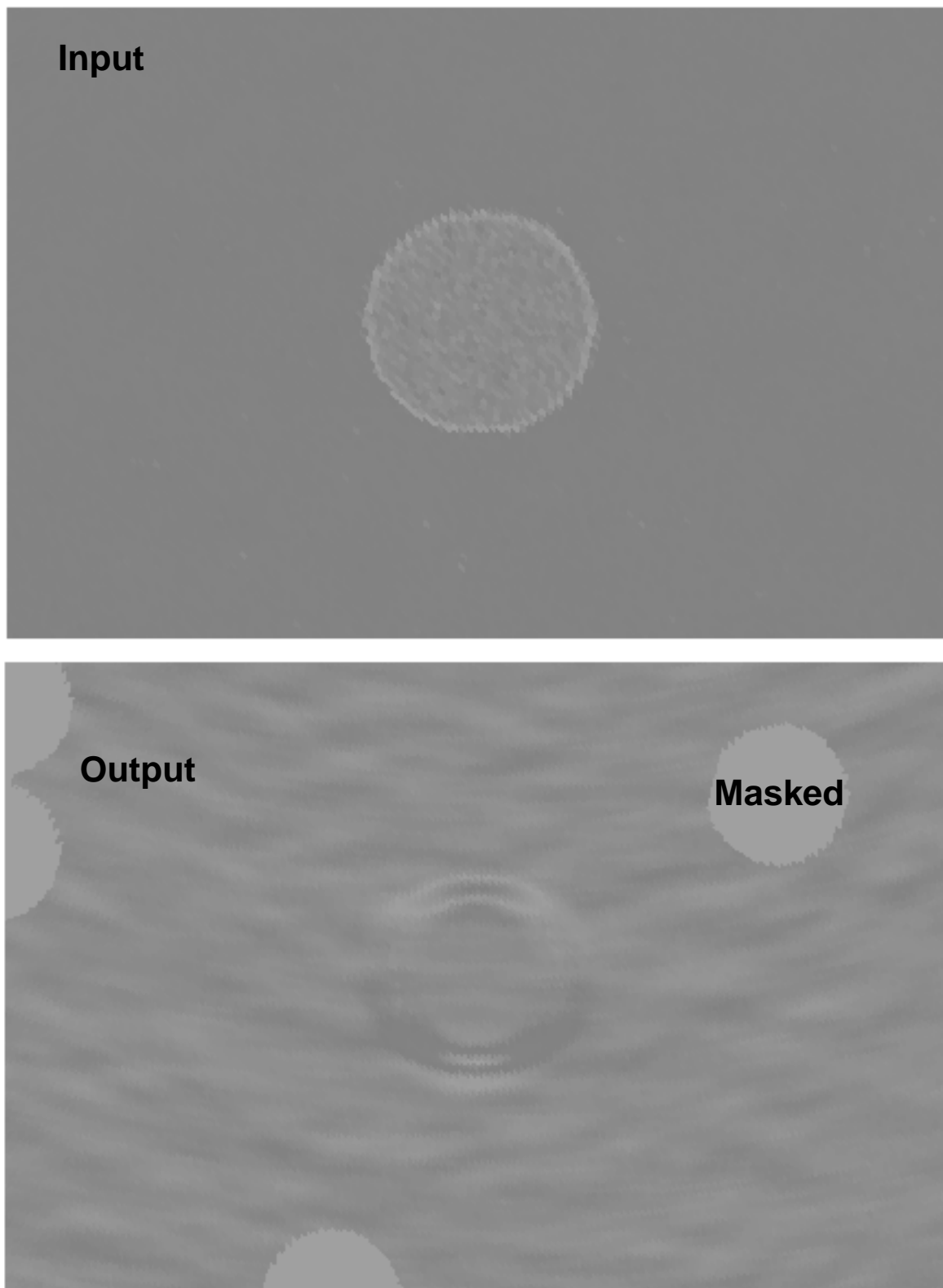


Fig. 2.— Edgfinder values around a string horizon. The Edgfinder is oriented North (up) to South (down). The light blue circles are masked pixels in the WMAP data due to foreground sources.

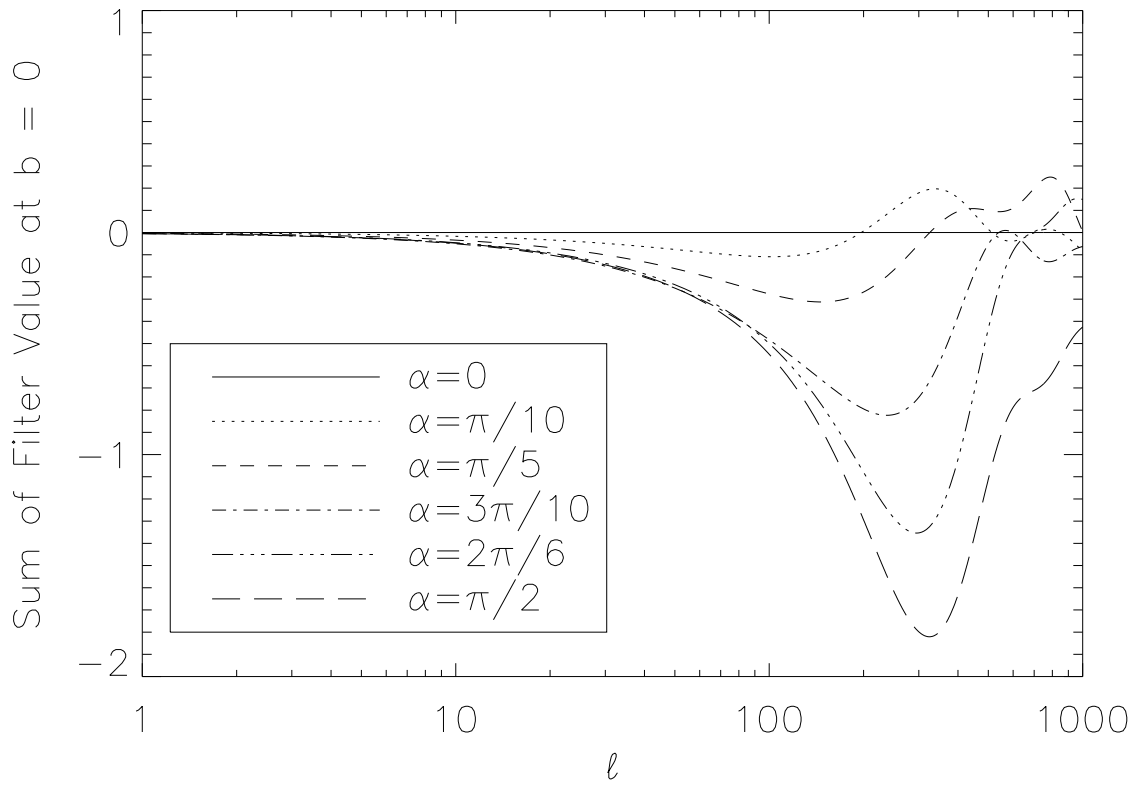


Fig. 3.— The response function of the Edgefinder Filter. Note the peak at  $\ell \sim 200$ , around where the first Doppler peak of the CMB anisotropy angular power spectrum occurs.

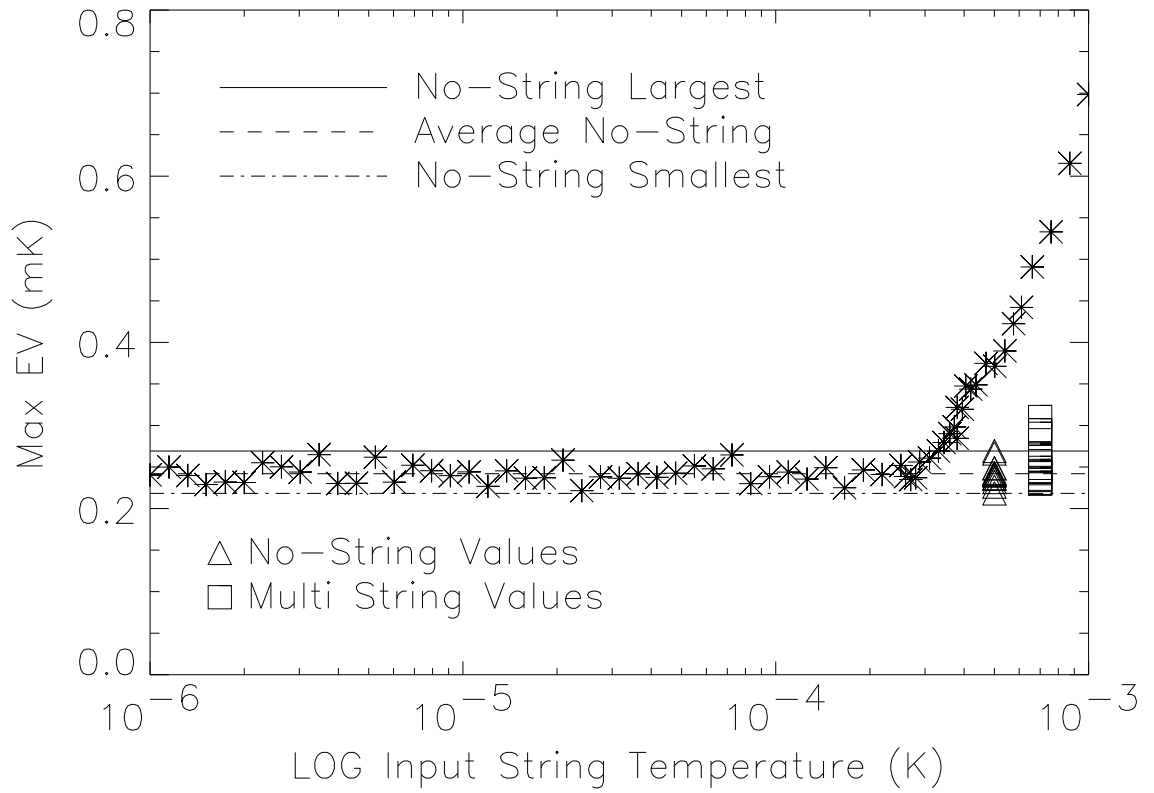


Fig. 4.— Plot of the input string temperature  $T_f$  vs. the maximum EV of the set.

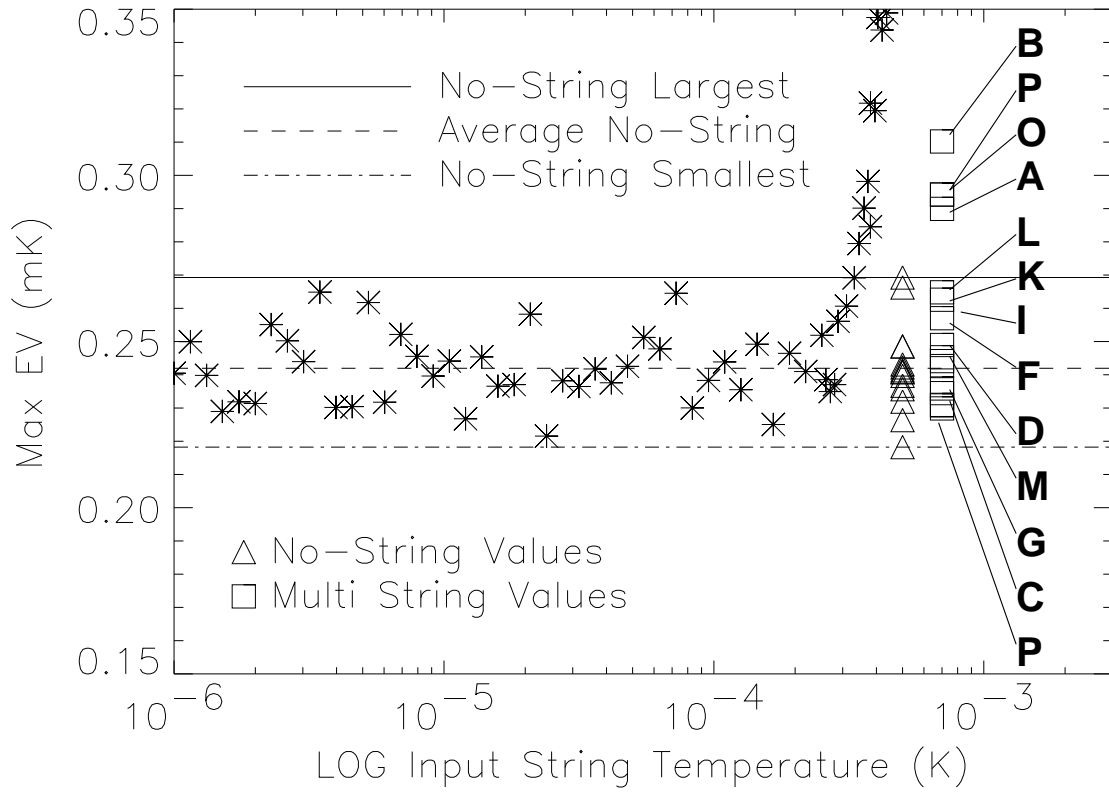


Fig. 5.— Detail of the plot of the input string temperature  $T_f$  vs. the maximum EV. Also plotted are the multi-string set data as well as limits from the No-String sets.

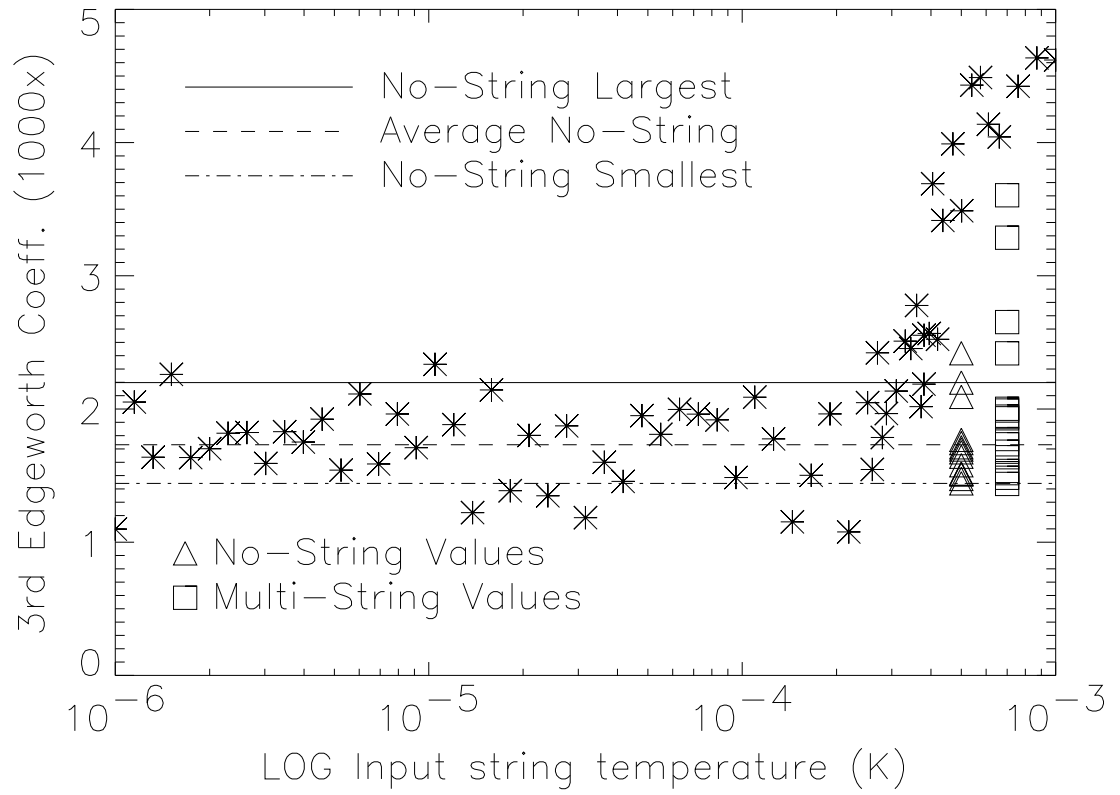


Fig. 6.— Plot of the input string temperature  $T_f$  vs. the 3rd Edgeworth coefficient.

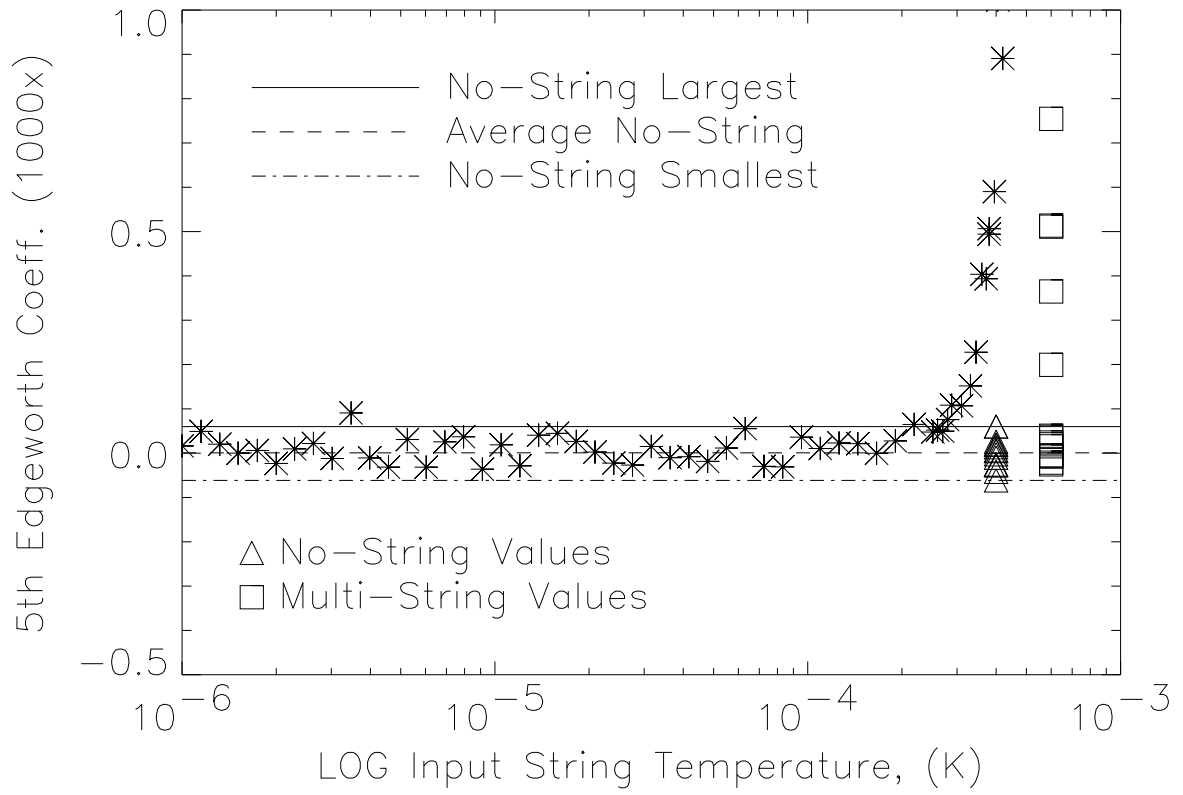


Fig. 7.— Plot of the input string temperature  $T_f$  vs. the 5th Edgeworth coefficient.

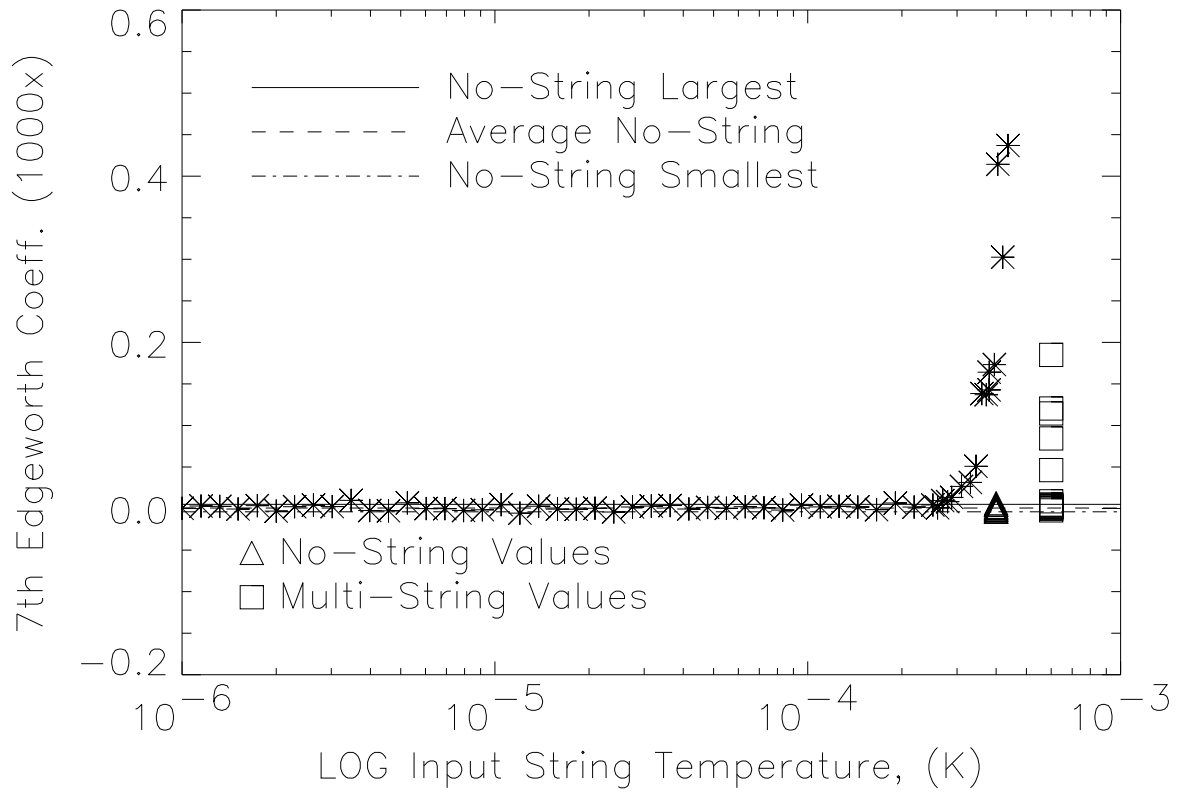


Fig. 8.— Plot of the input string temperature  $T_f$  vs. the 7th Edgeworth coefficient.

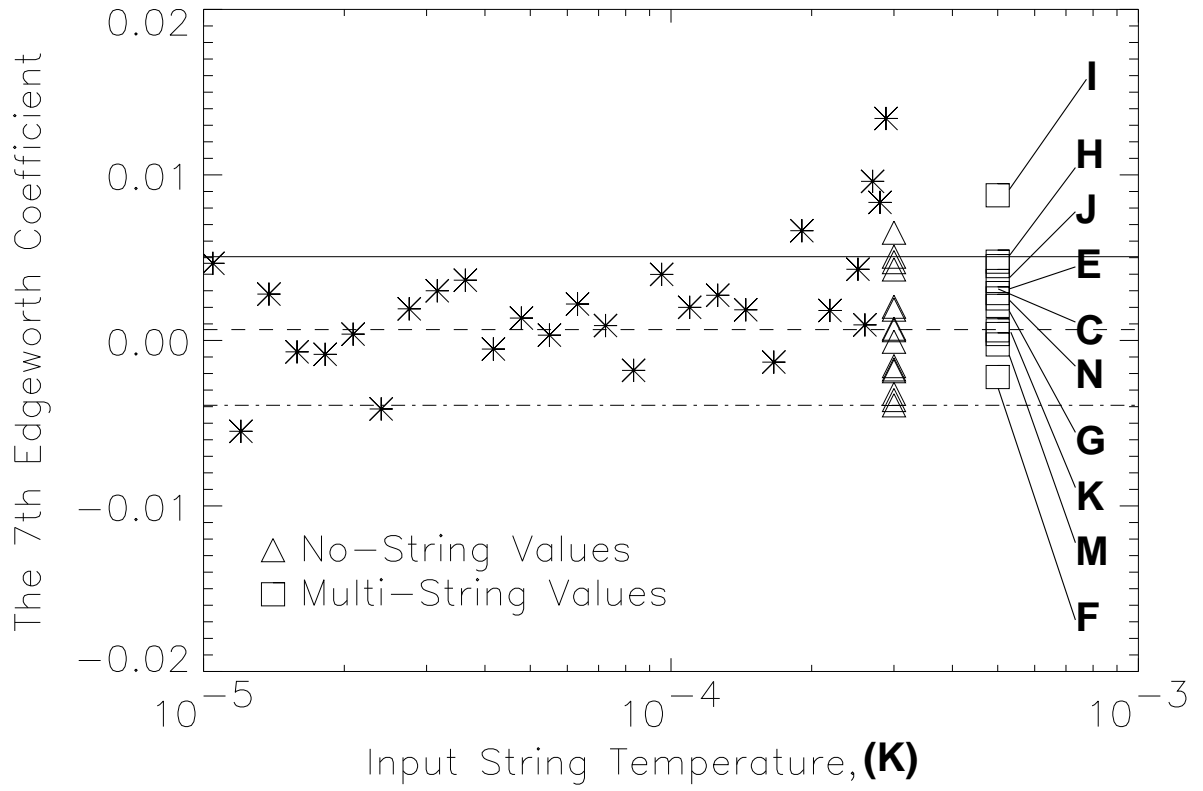


Fig. 9.— Detail of the plot of the input string temperature  $T_f$  vs. the 7th Edgeworth coefficient. Also plotted are the multi-string set data as well as limits from the No-String sets.

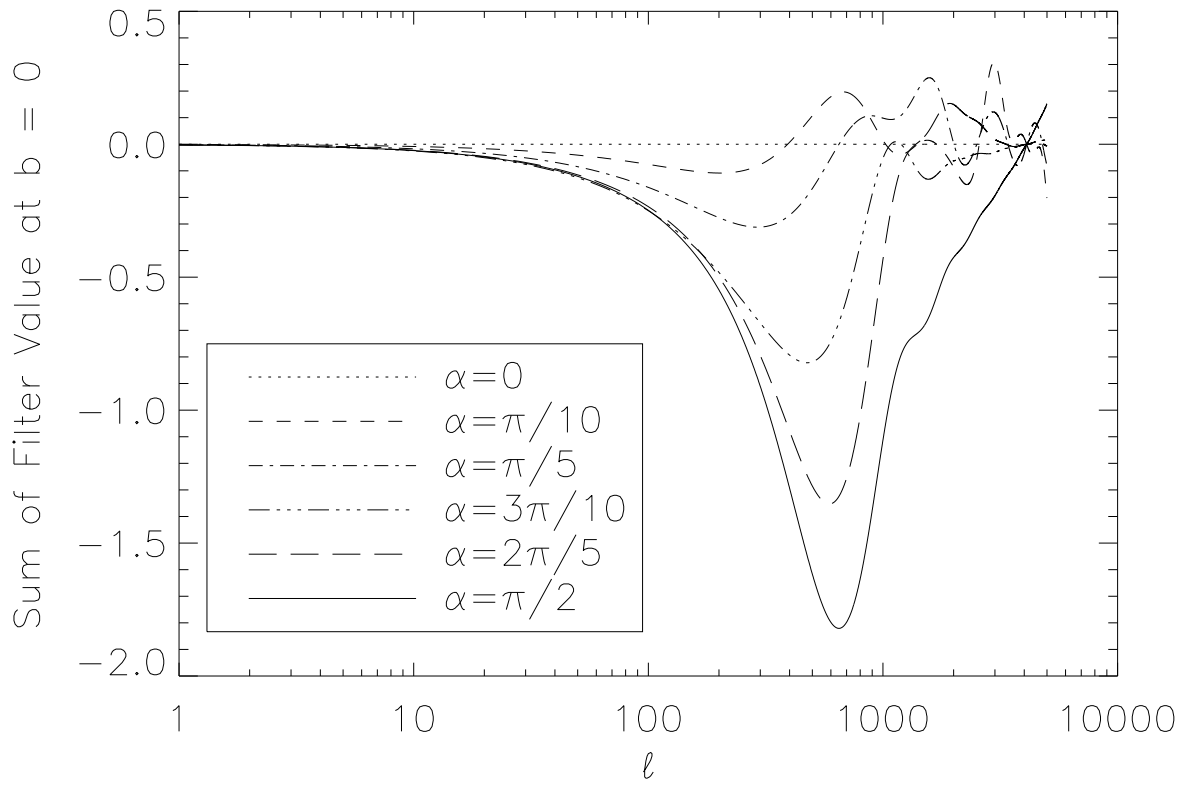


Fig. 10.— Transfer function for the PLANCK simulation; the filter had  $RAD = 0.5$ .

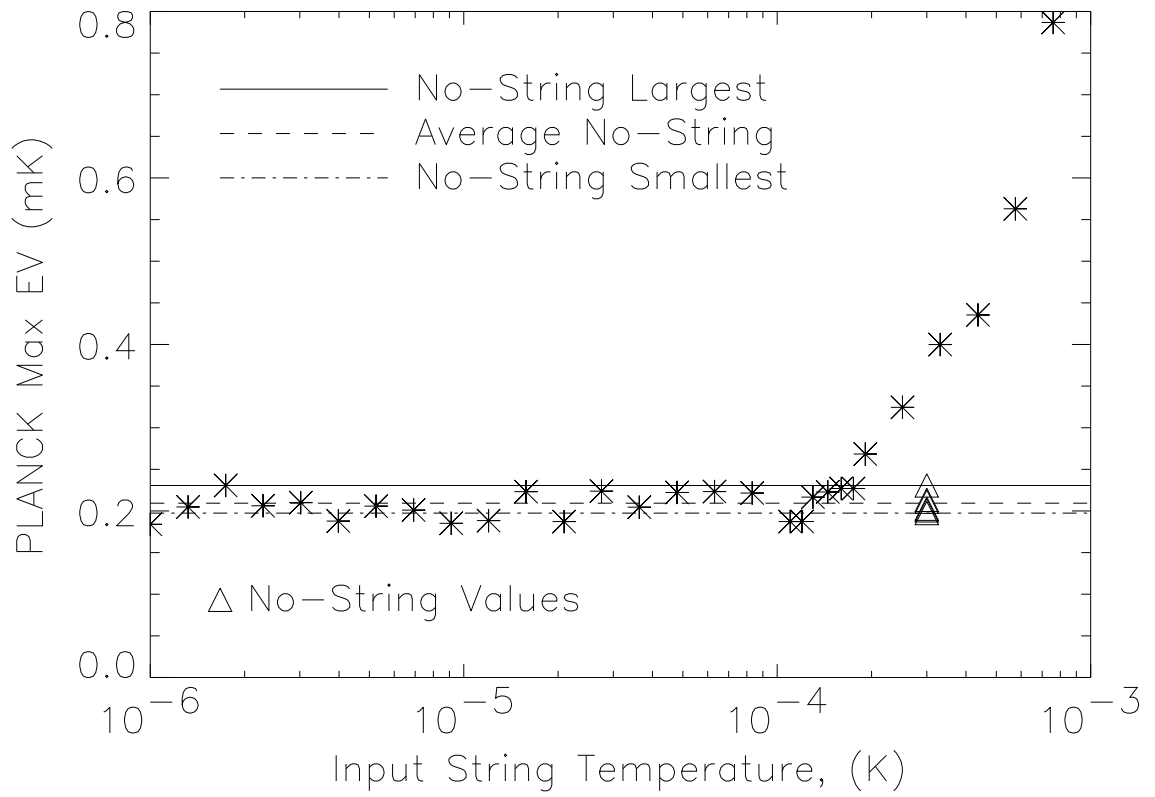


Fig. 11.— Input string temperature vs. the maximum EV of the EV set for simulated PLANCK data.

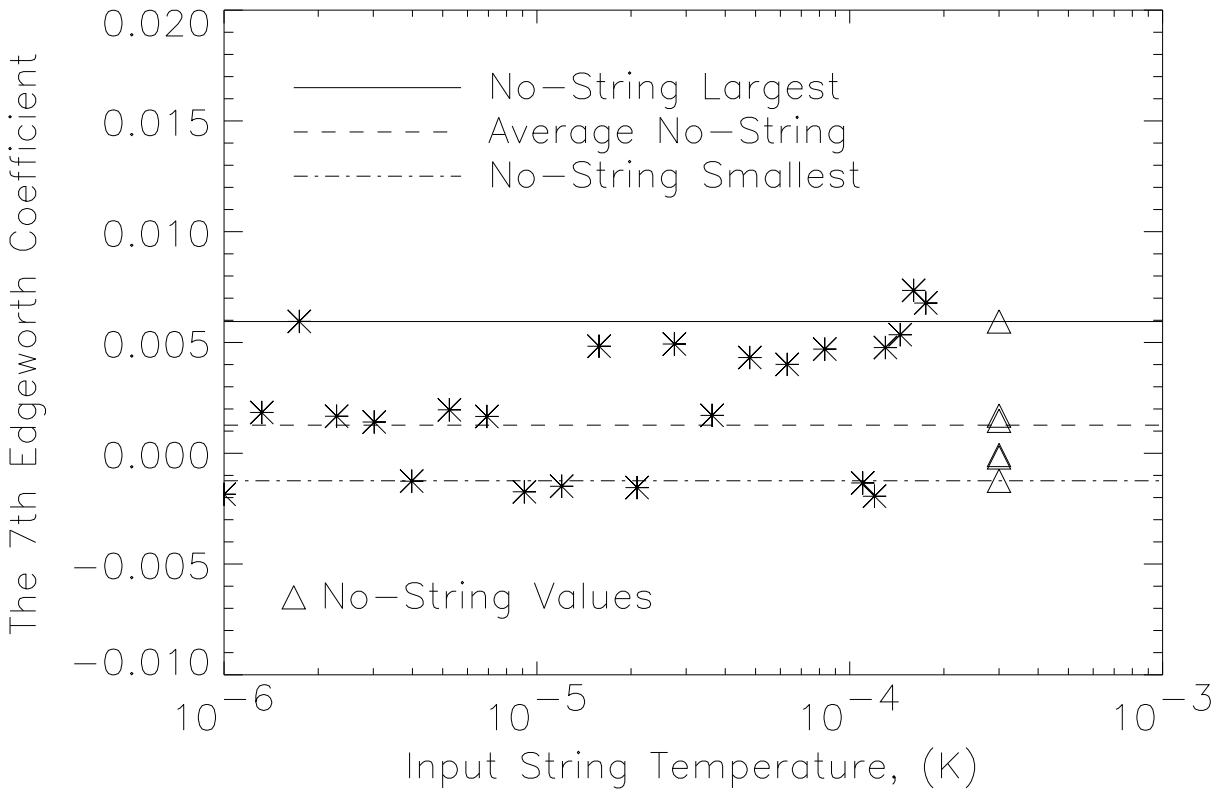


Fig. 12.— Blow up of input string temperature vs. the 7th Edgeworth coefficient of the EV set for simulated PLANCK data.

Table 3. Edgefinder Gain Calibration

$T_s^a$	EV Gain $_{ \alpha=0}^b$	EV Gain $_{ \alpha=\pi/2}$
1.000000	0.9567	0.9956
0.100000	0.9985	0.9732
0.010000	1.0800	0.9085
0.005000	0.8456	0.9630
0.001000	0.7639	1.0150
0.000500	0.8046	0.9842
0.000100	0.9296	0.8974
0.000050	0.8974	0.9794
0.000010	0.9559	1.0200
0.000001	1.0440	1.0910

<sup>a</sup> $T_s$  is the input cosmic string horizon temperature

<sup>b</sup>EV Gain is  $-\text{EV}/T_s$ , here quoted for 2 different  $\alpha$  angles.

Table 4. Number and Strength of Input Strings for Multi-String Simulated Maps.

Data Set	# of Strings	$RAD$	$T_s$	Max. EV	$E_7(10^{-6})$
<b>Multi A</b>	2	2.0	0.30	0.290	84.4
<b>Multi B</b>	4	2.0	0.30	0.310	185
Multi C	10	2.0	0.030	0.231	2.86
Multi D	4	2.0	0.030	0.236	−2.21
Multi E	30	2.0	0.030	0.257	3.59
Multi F	60	2.0	0.030	0.243	−2.42
Multi G	5	2.0	0.015	0.231	2.09
Multi H	10	2.0	0.015	0.245	4.76
<b>Multi I</b>	20	2.0	0.15	0.244	8.77
Multi J	2	4.0	0.015	0.249	4.49
Multi K	2	4.0	0.030	0.263	0.609
<b>Multi L</b>	2	1.0	0.30	0.265	46.2
Multi M	5	2.0	0.15	0.234	0.394
Multi N	10	2.0	0.15	0.230	2.54
<b>Multi O</b>	5	1.0	0.30	0.294	120
<b>Multi P</b>	10	1.0	0.30	0.294	114

Table 5. Select Properties of the WMAP composite QVW Data.

WMAP Band	Max Map T	Max EV	$E_7$
QVW	0.666	0.258	$-3.82 \times 10^{-6}$

Table 6. Edgfinder Values for CSL-1

Pixel #	WMAP QVW T	$EV _{\alpha=0}$ /%-tile	$EV _{\alpha=\pi/20}$ /%-tile
968549	-0.144015	0.07336 / 95.30%	0.08686 / 97.61%
968550	-0.0735366	0.08322 / 97.11%	0.08280 / 97.05%
968548	0.0418802	0.1248 / 99.76%	0.08621 / 97.53%
968527	0.0717491	0.1234 / 99.74%	0.09720 / 98.65%

Note. — EV of CSL-1 and 3 immediately adjacent pixels. Values listed are for  $\alpha = 0$  and  $\alpha = \pi/20$